Available online at www.sciencedirect.com
ScienceDirect
Journal of Power Sources 178 (2008) 692–698
JOURNAL OF POWER SOURCES
www.elsevier.com/locate/jpowsour

Heat transport characteristics of flow fields in proton exchange membrane fuel cells

Son Ah Cho, Pil Hyong Lee, Sang Seok Han, Sang Soon Hwang *

Department of Mechanical Engineering, University of Incheon, Dohwa-dong 177, Nam-gu, Incheon 402-749, South Korea

Received 27 June 2007; received in revised form 7 August 2007; accepted 12 September 2007
Available online 26 September 2007

Abstract

Since the electrochemical reaction at electrodes of PEMFC is a form of exothermic reaction, three-dimensional non-isothermal numerical simulation was developed including the energy equation with all heat source terms such as reversible heat generation and irreversible heat release attributed to ohmic and activation polarization. The results show that the maximum temperature is observed at the cathode because of reaction heat from water formation reaction and temperature at the electrolyte along channel increases due to accumulative heat addition and heat is mainly generated by irreversible loss at a low voltage and by water formation loss at a low current density.

Keywords: PEM fuel cells; Temperature distribution; Energy equation; Source term

1. Introduction

Since the electrochemical reaction at the anode and cathode electrodes of a polymer membrane electrolyte fuel cell (PEMFC) is a form of exothermic reaction, the interior temperature of the fuel cell increases as operation time lapses. In general, PEMFC performance improves as gas humidity increases because the humidity enhances mobility of hydrogen ions across the polymer electrolyte. In this respect, any increase of temperature by reaction heat which can make the humidity of reactant gases lower could cause a worsening of fuel cell performance. On the other hand, a higher operating temperature helps to enhance the electrochemical reaction rate, leading to a production of high current in the fuel cell. Therefore, to assure optimal performance of the PEMFC and provide proper heat management of the fuel cell, it is of crucial importance to investigate the heat transfer characteristics of fuel cell. Many studies have been carried out to analyze the heat transfer characteristics of PEMFC experimentally and numerically. Nguyen and White [1], Fuller and Newman [2] simulated numerically two-dimensional membrane electrode assembly to examine the heat and water management of fuel cell. They concluded thermal control is critical to the performance of PEMFC and heat transfer requirement changes with current density. Shimpalee and Dutta [3] developed three-dimensional model including energy equation to predict the temperature distribution inside flow channel. Their results showed the fuel cell performance depends on the temperature rise inside fuel cell. Rowe [4] compared the temperature difference with increasing current density using energy equation with irreversible, reversible and ohmic resistance. They found that temperature distribution within the PEM fuel cell is affected by water phase change in the electrode. Hwang and Chen [5] used energy equation applying local non-equilibrium condition and Ju et al. [6] and Zhou and Liu [7] included irreversible reaction heat into energy equation to describe more realistic temperature distribution inside fuel cell. Berning et al. [8] developed non-isothermal three-dimensional numerical model incorporating entropy change and irreversibility due to the activation overpotentials to find out temperature gradient within the cell. Nguyen [9] accounted for heat generation due to the electrochemical reaction for energy equation and analyzed the effects of concentration, temperature and ohmic overpotential at low and high load condition. Ying [10] investigated the effects of flow configurations on heat transfer in gas area and the solid land and Rajani [11] analyzed the performance of a vertical planar H2-air PEMFC under various operating conditions by

* Corresponding author. Tel.: +82 32 770 8417; fax: +82 32 770 8410.
E-mail address: hwang@incheon.ac.kr (S.S. Hwang).

0378-7753/$ – see front matter © 2007 Elsevier B.V. All rights reserved.
doi:10.1016/j.jpowsour.2007.09.057

Nomenclature

A_{cv}	specific surface area of the control volume (m^{-1})
D_w	diffusion coefficient of water ($m^2\,s^{-1}$)
F	Faraday constant, 96,487 C mol^{-1}
I	local current density ($A\,m^{-2}$)
k	thermal conductivity ($W\,(m\,K)^{-1}$)
M	molecular weight ($kg\,mol^{-1}$)
$M_{m,\,dry}$	equivalent weight of a dry membrane ($kg\,mol^{-1}$)
n	number of electrons in electrochemical reaction
n_d	electro-osmotic drag coefficient
P	pressure (Pa)
T	temperature (K)
$\vec{u}$	velocity vector ($m\,s^{-1}$)

Greek letters

α	transfer coefficient
ε	porosity
κ	ionic conductivity ($S\,m^{-1}$)
λ	water content in the membrane
μ	dynamic viscosity $(kg\,(m\,s)^{-1}$
ρ	density of the mixture ($kg\,m^{-3}$)
$\rho_{m,\,dry}$	density of a dry membrane ($kg\,m^{-3}$)

Superscripts

eff	effective value in porous region
ref	reference condition

using a 2D, steady state, single phase, non-isothermal and complete fuel cell model involving both flow and electrochemistry. Li [12] described thermodynamic concept of heat generated by reversible and irreversible reaction. Alazmi and Vafai [13] investigated the effect of interfacial condition between porous media and fluid flow to velocity and temperature and Nusselt number. They found that variation of interfacial condition have a more pronounced effect on the velocity field rather than temperature field. Yuan et al. [14,15] have simulated and analyze systematically using full three-dimensional calculation methods to present gas flow and heat transfer characteristics in terms of friction factor and Nusselt number. They showed the duct configuration and properties of the porous anode layer have significant effects on both gas flow and heat transfer in fuel cell.

The previous research described above did not take into consideration all energy source terms such as ionic resistance loss, reversible and irreversible loss, and water formation loss which directly affects the interior temperature of PEMFC. Consequently, the results had some limitations in realistically predicting temperature distribution and heat generation inside fuel cells.

In this paper, a three-dimensional non-isothermal numerical simulation of the PEMFC was developed, including an energy equation with all heat source terms, such as heat generation due to entropy change from electrochemical reaction, and irreversible heat release attributed to ohmic and activation polarization, as well as heat released by water formation. The purpose of this study is to investigate the contribution of each

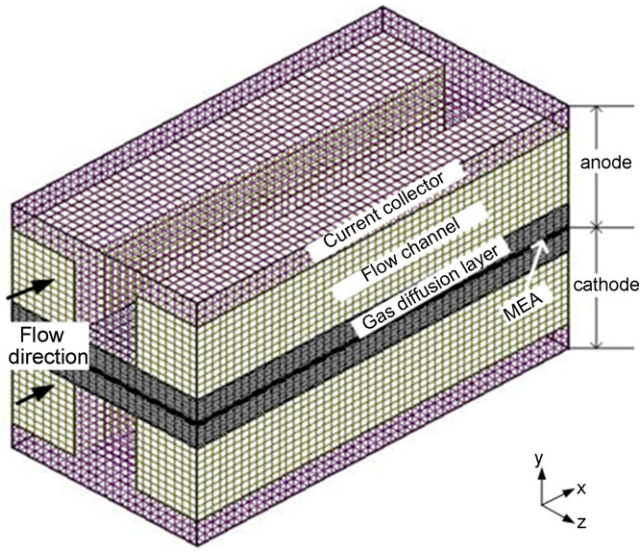

Fig. 1. Mesh configuration of the numerical PMFC model with a single flow channel.

source term on heat generation and temperature distribution; and contribution of energy source terms according to a change in the current density. This study also analyzes how current density affects the Nusselt number, a parameter essential to heat transfer. This work could provide basic data for the design of the heat and water management of polymer electrolyte fuel cells.

2. Computational methods

Three-dimensional, non-isothermal, steady state model is used for simulating PEMFC in this work. Computational mesh which consists of anode flow channel, anode diffusion layer, anode catalyst layer, MEA, cathode catalyst layer, cathode diffusion layer and cathode flow channel is depicted in Fig. 1. In this model, the flow direction at anode and cathode flow channel is set to be same, called as co-flow condition. Cell design parameters and cell operating conditions are described at Table 1. Number of mesh is about 60,000 and average number of iterations for

Table 1
Cell design parameters and cell operating conditions

Description	Value
Cell/electrode length (cm)	10
Gas channel height (cm)	0.12
Gas channel width (cm)	0.08
Anode GDL thickness (cm)	0.0375
Porosity of anode GDL	0.7
Membrane thickness (cm)	0.01
Catalyst layer thickness (cm)	0.0025
Porosity of cathode GDL	0.7
Cathode GDL thickness (cm)	0.0375
Cell temperature (K)	353
Pressure at the anode gas channel inlet (atm)	1
Relative humidity of inlet fuel stream (%)	100
Anode stoichiometry	2
Pressure at the cathode gas channel inlet (atm)	1
Cathode stoichiometry	3
Cell voltage (V)	0.6
Inlet nitrogen–oxygen mole fraction ratio	0.79/0.21

converged solution is about 10,000. Xeon^{TM} CPU 2.8 GHz PC was used for calculation in this work.

2.1. Governing equations

Mass (1), momentum (2), species (3) and energy (4) equation for reactive fluid flow is as follows:

$$\nabla(\varepsilon\rho u) = S_{\mathrm{m}} \tag{1}$$

$$\nabla(\varepsilon\rho\vec{u}\vec{u}) = -\varepsilon\nabla p + \nabla(\varepsilon\mu\nabla\vec{u}) + S_{\mathrm{u}} \tag{2}$$

$$\nabla(\varepsilon\vec{u}C_{\mathrm{k}}) = \nabla(D_{\mathrm{k}}^{\mathrm{eff}}\nabla C_{\mathrm{k}}) + S_{\mathrm{k}} \tag{3}$$

$$\nabla(\varepsilon\vec{u}h) = \nabla(k\nabla T) + S_{\mathrm{h}} \tag{4}$$

The source terms in energy equation expresses heat generations as follows:

$$(E_{\mathrm{r}}(T, P) - V_{\mathrm{cell}})I(x, y, z)A_{\mathrm{cv}} \tag{5}$$

$$-T\frac{\partial E_{\mathrm{r}}}{\partial T}I(x, y, z)A_{\mathrm{cv}} \tag{6}$$

$$\frac{I^2(x, y, z)}{\kappa^{\mathrm{eff}}}A_{\mathrm{cv}} \tag{7}$$

Irreversible heat generation (5) is attributed to activation and ohmic overpotential. Reversible heat generation (6) comes from the entropy change of overall reaction, $H_2 + O_2/2 \rightarrow H_2O$. And ionic resistance loss (7) is generated by resistance of movement of ions across membrane. Water formation reaction heat can be expressed as follows:

$$\Delta h_{\mathrm{H_2O}}\frac{1 + 2\alpha}{2F}I(x, y, z)M_{\mathrm{H_2O}}A_{\mathrm{cv}} \tag{8}$$

E_{r} is reversible cell potential as follows:

$$E_{\mathrm{r}}(T, P) = -\frac{\Delta G(T, P)}{nF} = E_{\mathrm{r}}(T_{\mathrm{ref}}, P) + \left(\frac{\Delta S(T_{\mathrm{ref}}, P)}{nF}\right)(T - T_{\mathrm{ref}}) \tag{9}$$

where G is free energy of H_2/O_2 reaction.

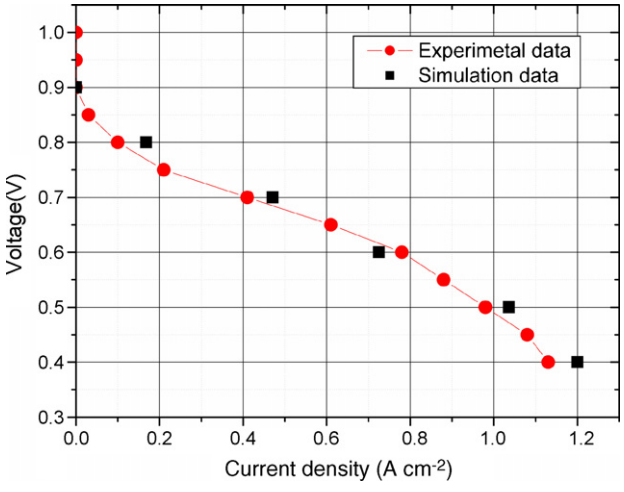

Fig. 2. Comparison of calculated results with the experimental data for *V–I* curve.

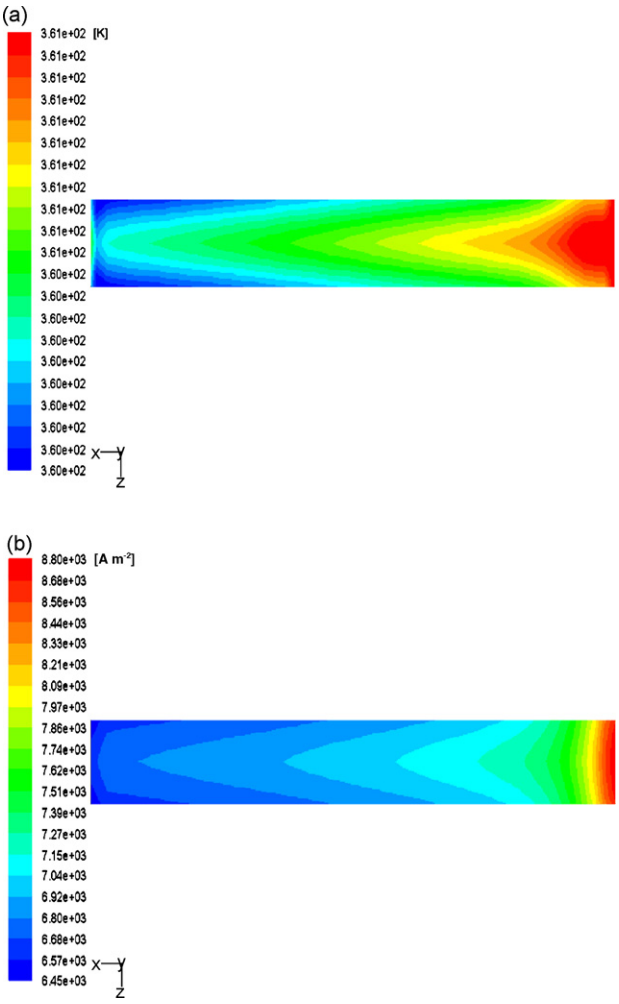

Fig. 3. Temperature (a) and local current density (b) distribution on the surface of membrane for 0.6 V.

Nusselt number of heated wall is defined by

$$Nu = \frac{qD_{\mathrm{h}}}{k(T_{\mathrm{w}} - T_{\mathrm{bulk}})} \tag{10}$$

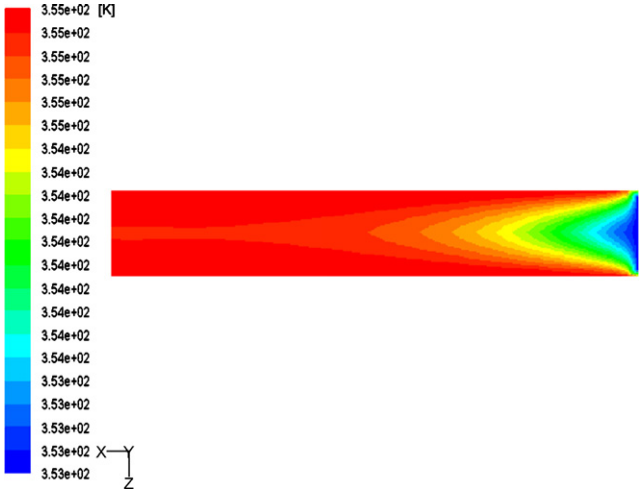

Fig. 4. Temperature profile on the middle cross-section of flow channel for 0.6 V.

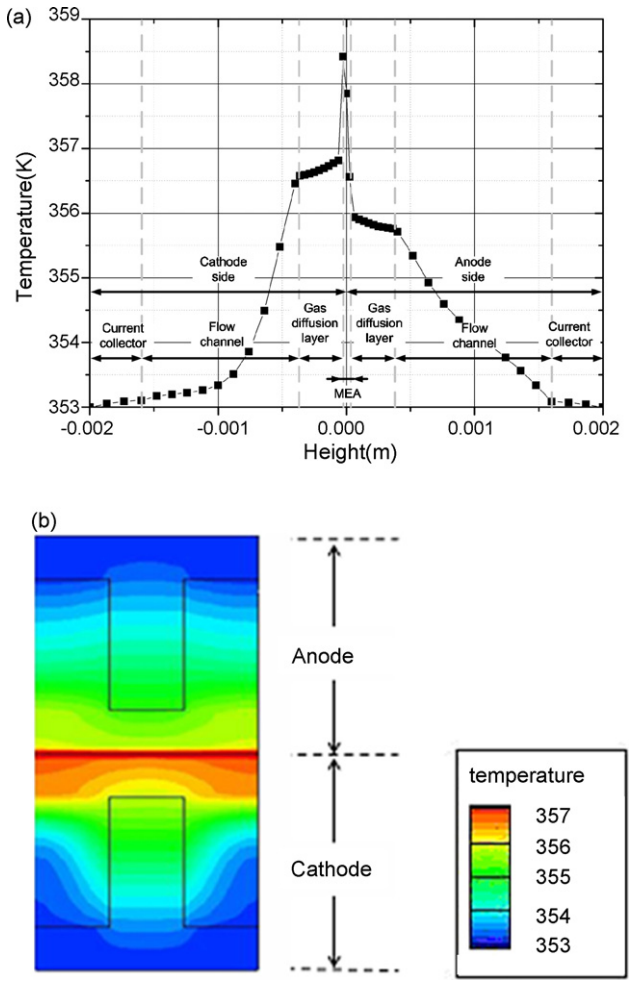

Fig. 5. Temperature profile (a) and temperature distribution (b) at the cross-section and the through plane direction for 0.6 V at $x = 0.09$ cm.

where T_{bulk} is the bulk flow mean temperature in the cross-section and calculated as

$$T_{\text{bulk}} = \frac{\int T|U|\mathrm{d}A}{\int |U|\mathrm{d}A} \tag{11}$$

Water transport through the membrane comprise of two different water transport processes: the electro-osmotic drag (12)

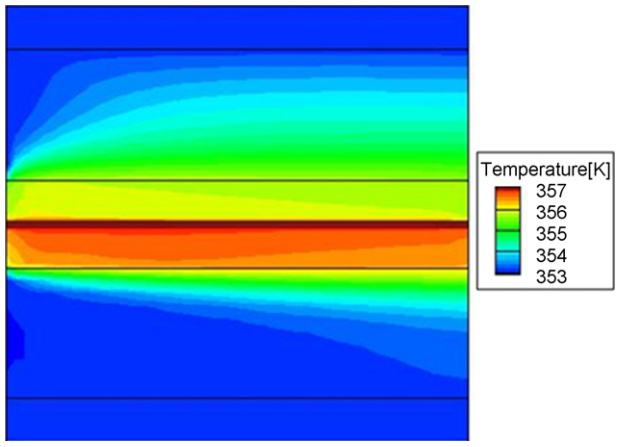

Fig. 6. Temperature distribution along the channel at symmetry surface for 0.6 V.

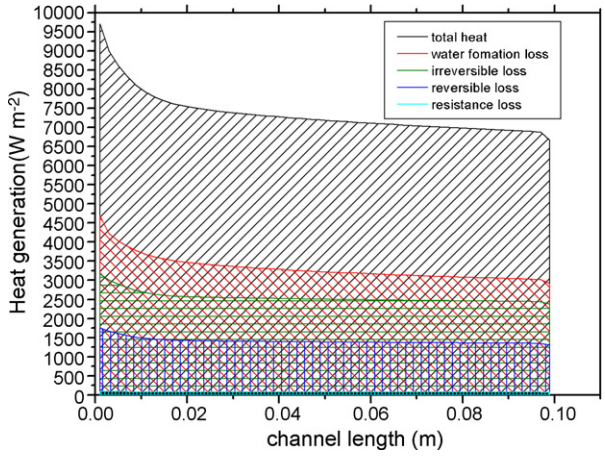

Fig. 7. Contribution of energy source terms to total heat generation for 0.6 V.

whereby hydrogen protons migrating through the membrane drag water molecules with them and back diffusion (13) of water from the cathode side to anode side.

$$J_{H_2O} = 2n_d \frac{I(x, y, z)}{2F} \tag{12}$$

$$J_{H_2O,\text{back diffusion}} = -\frac{\rho_{m,\text{dry}}}{M_{m,\text{dry}}} D_w \frac{\mathrm{d}\lambda}{\mathrm{d}z} \tag{13}$$

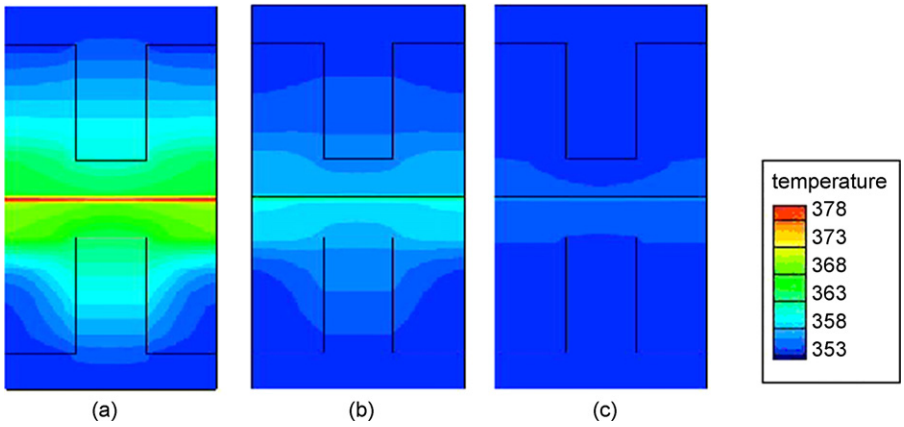

Fig. 8. Variation of temperature profile along the through plane of channel at different voltage conditions (0.2 V (a), 0.5 V (b) and 0.8 V (c)).

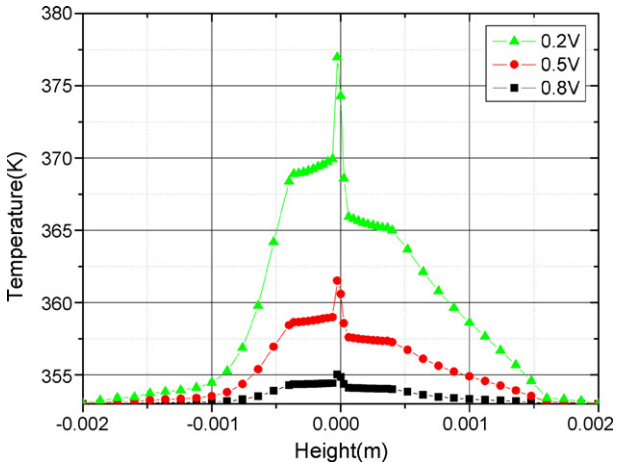

Fig. 9. Variation of temperature profile at cross-section for 0.2 V, 0.5 V, and 0.8 V.

3. Discussions

To provide a validation check of the numerical model, the experimental performance results of PEMFC(12) with the parallel flow channel and the computational results, are compared as shown in Fig. 2. The performance curve derived from the numerical simulation agrees with experiments and represents reasonable overvoltage levels for entire regions of current density. To see how the temperature inside of a fuel cell is distributed by the electrochemical heat generation in each electrode, the temperature distribution on the membrane surface of the fuel cell at the nominal operating condition, 0.6 V, is shown in Fig. 3(a). The temperature tends to become higher at the flow entrance and near the middle region. It is thought that this high temperature at entrance region is caused by high concentration of hydrogen and oxygen supplied at the flow inlet. This temperature distribution is similar to the distribution of local current density in Fig. 3(b) since local current density is closely dependent on electrochemical reaction rate proportional to concentration of reactants, e.g. hydrogen and oxygen. It is important to know local temperature profile inside flow channel because the temperature of reactant flowing inside flow channel can affect greatly electrochemical reaction rate. Fig. 4 shows temperature distribution at the symmetry plane in the flow channel along the flow direction. It is found that the temperature of reactants inside flow channel gradually rises along the flow direction due to the accumulation of heat generated at each electrode.

Fig. 5(a) shows the temperature profile of the through plane direction of a flow channel at 0.6 V. In the figure, the left side is a cathode and the right side is an anode. Approaching to the

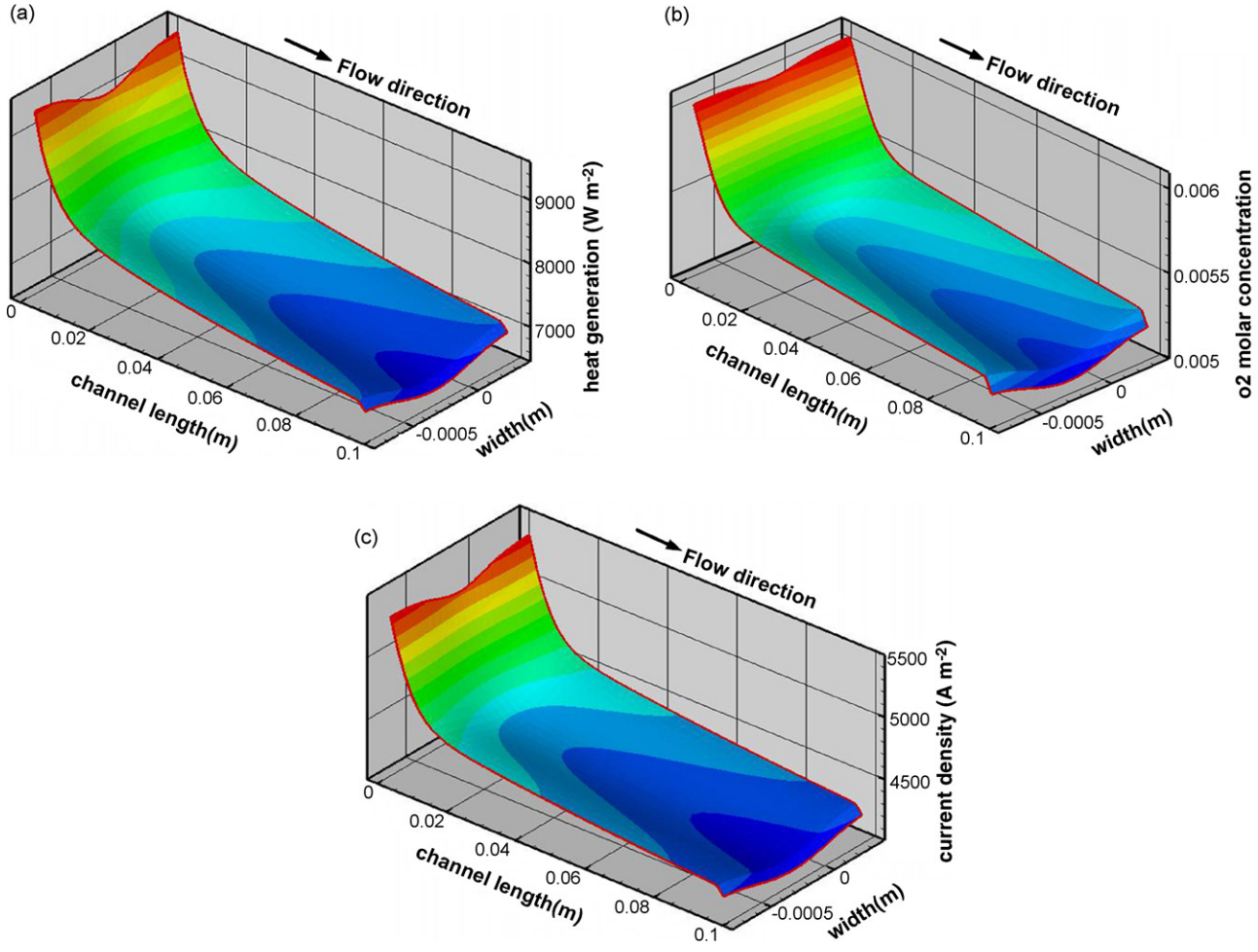

Fig. 10. Heat generation (a) and oxygen (b) and current density (c) along the flow channel for 0.6 V.

catalyst layer, the temperature becomes higher. In particular, the temperature peak is found at the cathode side, which means that the water formation reaction by hydrogen and oxygen on the cathode catalyst layer generates a large amount of heat. The difference between the membrane surface and the maximum temperature in the channel is about 3°.

Fig. 5(b) shows the temperature distribution at a cross-section, including the current collector, flow channel and MEA. The temperature in the flow channel at the cathode side is found to be spatially higher. On the other hand, the temperature at the current collect is uniform because of the high heat conductivity coefficient of the current collect. Fig. 6 shows the temperature distribution at a middle section of the flow channel at an anode and a cathode. It reveals that the temperature rises along the flow path, and especially the high temperature zone is distributed in the gas diffusion layer of the cathode. Fig. 7 represents each energy source term along the flow path in order to examine the contribution of each energy source term on heat generation. In the figure, it is found that heat generation by water formation loss is the largest, followed by irreversible loss and reversible loss for 0.6 V condition.

Since the current density of fuel cells increases with decreasing voltage, it is important to examine temperature distribution at different voltages.

Fig. 8 shows the temperature profiles of the through plane direction of flow channels at different voltages. The temperature difference at 0.2 V is greatest where the current density appears high, and the temperature at 0.8 V is spatially very low because the electrochemical reaction rate is not very active. Fig. 9 shows the temperature distribution of a cross-section plane at each voltage, which also helps explain why the lower the voltage is, the higher the temperature appears.

Fig. 10 presents heat generated by an electrochemical reaction, an oxygen profile and current density along the flow path. From Fig. 10(a) the heat decreases sharply at inlet and then maintains a certain level to the exit. It is postulated that chemical reactions are more active near the entrance where reactant gases flow in, and reactant concentration is high. To validate this, the oxygen concentration was plotted along the flow direction in Fig. 10(b). It shows that the oxygen concentration sharply decreases near the entrance, but maintains a certain level along the length direction. The current density which represents the electrochemical reaction rate, also shows a similar trend along the flow path, as shown in Fig. 10(c).

Fig. 11 compares each energy source consisting of heat generation with varying voltage. It is found that at 0.2 V heat generation due to irreversible loss is the largest where the current density is highest, and heat generation by irreversible loss decreases at 0.5 V, and then heat generation by water forma-

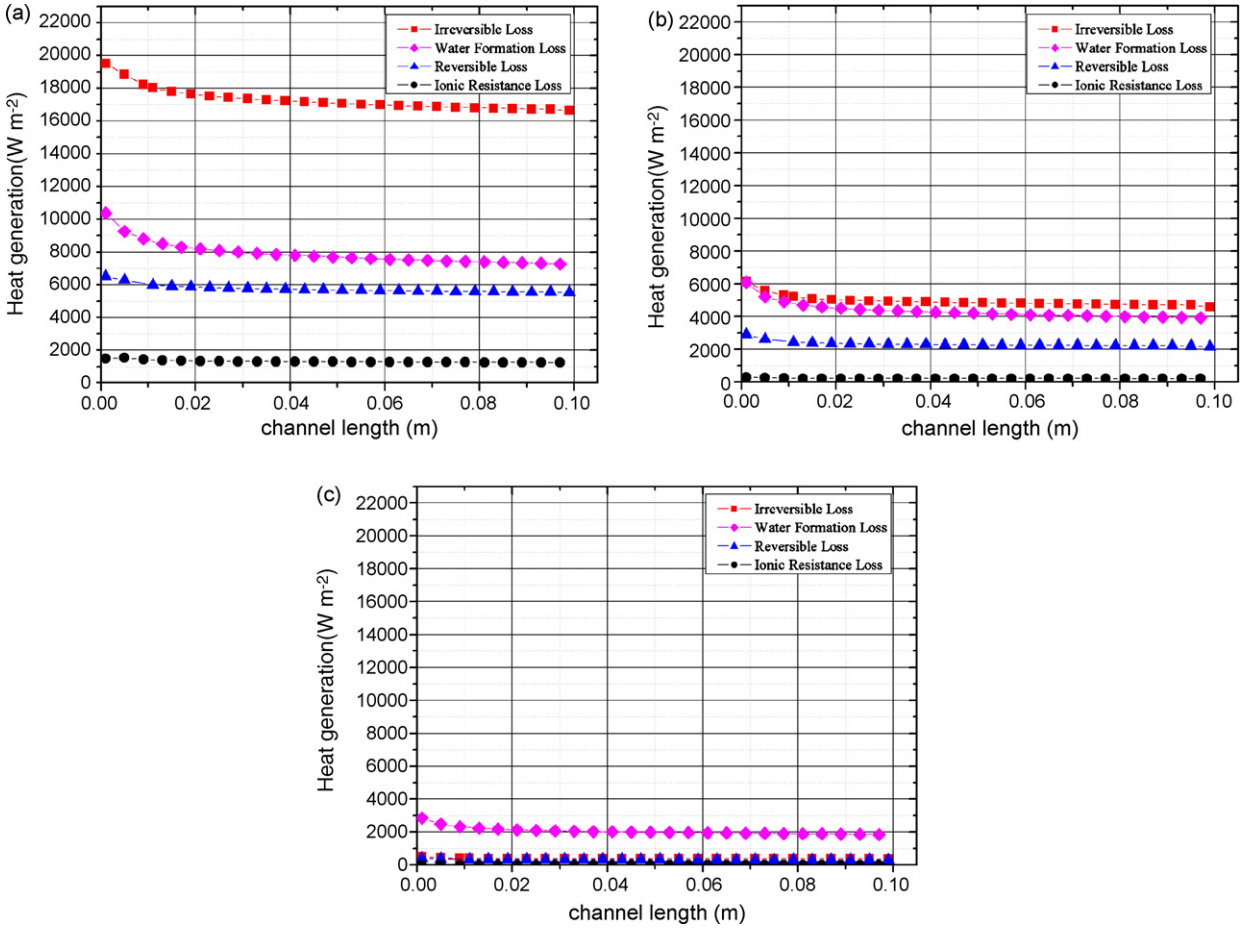

Fig. 11. Comparison of each source terms for different voltage conditions (0.2 V (a), 0.5 V (b) and 0.8 V (c)).

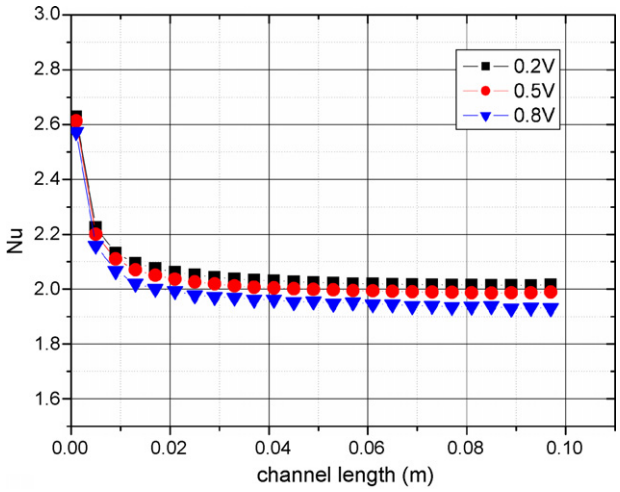

Fig. 12. Comparison of Nusselt number for 0.2 V, 0.5 V, and 0.8 V.

tion loss becomes the largest of all at 0.8 V where the current density is lowest. This is due to the fact that heat generation by irreversible loss increases because of the increase of overvoltage at a high current density. It is also found that at a low current density the heat generation by reaction heat and reversible loss is relatively greater than the heat generation by irreversible loss, since overvoltage is decreased at a low current density. Such a trend can be found through the comparison of energy source terms according to voltage shown in Fig. 11. Water formation loss, ionic resistance loss and reversible loss do not change much according to voltage, but heat generation by irreversible loss changes greatly according to the voltage applied. It is very important to control heat generation by irreversible loss at mid-high current density ranges for the proper heat transfer management of PEMFC.

Fig. 12 shows the Nusselt number along the flow direction at 0.2 V, 0.5 V and 0.8 V. It presents the shape of the rapid decay along the length direction. It is thought that this rapid decay of the Nusselt number along the flow axis is caused by the thermodynamic boundary layer development. It is also found that the Nusselt number increases with a decrease in voltage because the amount of heat generation rises at a high current density.

4. Conclusions

1. The maximum temperature is observed at the cathode because of heat generation from water formation reaction and temperature at the electrolyte along channel increases due to accumulative heat addition.
2. As the voltage decreases, the temperature difference between the flow and the electrodes increases due to the high electrochemical reaction rate at a high current density.
3. It is found that heat is mainly generated by irreversible loss at a low voltage and, on the other hand, by water formation loss at a low current density.
4. The Nusselt number increases with an increasing current density leading to higher heat generation. The rapid decay in the entrance of the channel is considered to be caused by thermal boundary layer development in the channel flow.

References

[1] T.V. Nguyen, R.E. White, J. Electrochem. Soc. 140 (1993) 2178–2186.
[2] T.F. Fuller, J. Newman, J. Electrochem. Soc. 140 (1993) 1218–1225.
[3] S. Shimpalee, S. Dutta, Numerical Heat Transf. Part A 38 (2000) 111–128.
[4] A. Rowe, X. Li, J. Power sources 102 (2001) 82–96.
[5] J.J. Hwang, P.Y. Chen, Int. J. Heat Mass Transf. 49 (2006) 2315–2327.
[6] H. Ju, H. Meng, C.-Y. Wang, Int. J. Heat Mass Transf. 48 (2005) 1303–1315.
[7] T. Zhou, H. Liu, Int. J. Trans. Phenom. 3 (2001) 177–198.
[8] T. Berning, D.M. Lu, N. Djilali, J. Power Sources 106 (2002) 284–294.
[9] P.T. Nguyen, T. Berning, N. Djilali, J. Power Sources 130 (2004) 149–157.
[10] W. Ying, T.-H. Yang, W.-Y. Lee, J. Ke, C.-S. Kim, J. Power Sources 145 (2005) 572–581.
[11] B.P.M. Rajani, A.K. Kolar, J. Power Sources 164 (2007) 210–221.
[12] X. Li, Principles of Fuel Cells, Taylor & Francis, New York, 2005.
[13] B Alazmi, K. Vafai, Int. J. Heat Mass Transf. 44 (2001) 1735–1749.
[14] J. Yuan, M. Rokni, B. Sundén, Int. J. Heat Mass Transf. 44 (2001) 4047–4058.
[15] J. Yuan, M. Rokni, B. Sundén, Int. J. Heat Mass Transf. 46 (2003) 809–821.